

## Analysis of the effect of keeper working conditions on hollow cathode performance

Feng Tian, Long Miao<sup>\*</sup>, Qimeng Xia, Fuwen Liang, Ningfei Wang, Xiao Hou

School of Aerospace Engineering, Beijing Institute of Technology, Beijing, 100081, China

### ARTICLE INFO

**Keywords:**

Hollow cathode  
Keeper working condition  
Emission characteristics  
Plume structure  
Discharge instability

### ABSTRACT

Hollow cathodes are widely used in electric thrusters due to their high emission electron density and low maintained voltage. The hollow cathode performance may significantly change under different keeper working conditions. In this study, a series of ground experiments were carried out to study the effects of the keeper current and the distance between keeper and cathode top on the emission characteristics and plume structure of the hollow cathode. The experimental results show that the working state of the keeper electronic circuit is less likely to be disturbed by the anode electronic circuit when the ratio of keeper current to anode current rises up. The plasma potential does not always rise up with the emission current in the far-field ( $>6$  cm) when the keeper current is not high ( $<3$  A). The extend of the distance between keeper and cathode top forms a high obstacle to the anode electronic circuit, this obstacle not only causes an increase of anode voltage, but also leads to a significant discharge instability of hollow cathode. In this case, a higher keeper current and xenon flow rate are required to keep a stable working state of hollow cathodes. The experimental results contribute to research on the discharge instability mechanism of hollow cathodes and provide useful information for instructing hollow cathode design.

### 1. Introduction

The hollow cathode discharge is a unique gas discharge in a cathode cavity, which has been widely used in ion thrusters [1–4], Hall-effect thrusters [5–8] and electric tether system [9–12]. As an important sub-component of the hollow cathode, the keeper is usually used for applying high voltage to ignite the hollow cathodes. After ignition, the keeper serves as a shield to reduce the heat loss and to protect the inner core from external plasma bombardment. Sometimes the keeper can also be used as a constant-current electrode for accurately fine-tuning the cathode performance.

The hollow cathode is a key component of the ion thrusters and Hall thrusters, so firstly it is necessary to find out its own discharge characteristics and performance using a simulated anode. Since the keeper electrode plays a significant effect on the working performance of hollow cathode, a great amount of the keeper-related research has been made. Domonkos [13] studied the effect of emission currents and xenon flow rates on the discharge characteristics of hollow cathodes. At lower gas flow rate and higher emission current, the keeper surface of the hollow cathode shows higher energy ion density, and the anode voltage

of the hollow cathode is larger. Byers [14] studied the effect of keeper current and keeper power supply impedance (different distances between keeper and anode) on the hollow cathode discharge characteristics. The anode voltage changes non-linearly with keeper current. Over the range tested (0.1–0.33 A), the maximum anode voltage is obtained at a keeper current of 0.20–0.25 A. The dependence of keeper and anode voltages on neutral flow rate under different keeper supply impedances are given, and an appropriate capacitive keeper circuit is superior to the resistive and inductive circuits on the basis of performance and control.

The keeper working conditions not only affect the discharge characteristics of the hollow cathode, but also lead to the discharge instability of hollow cathode and keeper corrosion. Meng [15] studied the effect of discharge current and keeper electron loss on discharge characteristics by axis in the main hollow cathode plume under different magnetic field intensities. The high oscillation amplitude of ionization instability in the cathode downstream region is found induced by the electron current loss on the keeper. The unstable discharge near the keeper will lead to serious wear of the hollow cathode, thus affecting its working performance [16,17]. Qin [18] studied the influence of gas flow rate, discharge current, and anode shapes on the oscillation

\* Corresponding author.

E-mail address: [miaolong@bit.edu.cn](mailto:miaolong@bit.edu.cn) (L. Miao).

characteristics of hollow cathode discharge. The spatial-temporal distributions of plasma potential, ion density, electron temperature, as well as the waveforms of plasma potential were measured. This high oscillation amplitude of plasma potential in the downstream sides of keeper outlet is known as “plume mode” instability ( $f = 10\text{--}150 \text{ kHz}$ ) [19]. The counter-interaction effects of rapid ionization of xenon atom and dissipation of xenon ion is considered as the main reason to form plasma pulse oscillation. Jorns [20,21] found that the oscillation amplitude of unstable discharge can be reduced by applying extra cold gas or external magnetic field. The high-frequency potential oscillation near the keeper electrode was first confirmed to be caused by ion acoustic turbulence (IAT) within an oscillation frequency  $f > 160 \text{ kHz}$  [19].

As can be seen that, the previous works have mainly focused on the influence of gas flow rate, discharge current, and external field environment on the discharge characteristics. However, until now, the information about the influence of keeper structural parameters and its working conditions on the discharge characteristics hollow cathode is relative few. Particularly, the study about the discharge instabilities of ionization and ion acoustic turbulence caused by the keeper has been still absent.

In this paper, a series of ground experiments are carried out to study the influence of the keeper current and distances between keeper and cathode top on the emission characteristics and plume structure of the hollow cathode. The relevance between the keeper and the discharge oscillations will be discussed. The experiment results about the hollow cathode working performances under different keeper working conditions could provide guidance for further hollow cathode design and working condition selection.

## 2. Experimental device system

**Fig. 1** shows the layout plan of the ground experiment equipment and the basic circuit connection plan. The hollow cathode emitter material is BaO-W, and the orifice diameter and the keeper outlet diameter are 0.6 mm and 5 mm respectively. The power supply required for hollow cathode operation includes heater power supply (40 V/20 A), keeper power supply (200 V/5 A) and anode power supply (120 V/8 A). The diagnostic and measuring systems include the Langmuir probes, current probes (Tektronix TCP0030A, with a measurement accuracy of  $\pm 0.1\%$ ), voltage probes (CYBERTEKP1300, with a measurement accuracy of  $\pm 0.1\%$ ), and digital oscilloscope (TeckMDO3014, with a

measurement accuracy of  $\pm 1\%$ ). The current and voltage probes are used to measure the keeper current, emission current, keeper voltage and anode voltage with a sampling rate of 100 MHz [5]. The discharge images of the hollow cathode are taken by a digital camera (Canon EOS 550D).

The origin point (0,0) of the measuring region of the Langmuir probe is located at the center of the keeper outlet. The Langmuir probe measurement of hollow cathode plume plasma is divided into near-field (0–6 cm), middle-field (6–48 cm) and far-field (48–84 cm) regions in axial direction, and the probes used in different regions are selected according to the plasma parameters. The diameter of the probes must be significantly larger than the plasma Debye length, otherwise it will cause large measurement errors. The plasma density of the hollow cathode plume ranges from  $10^{17} \text{ m}^{-3}$  to  $10^{13} \text{ m}^{-3}$ , which requires a large change in the diameters of the probes. As a first approximation, the electron temperature is assumed to be 3 eV, and the equivalent diameter is chosen to be 10 times the Debye length [22]. Therefore, three probes of different sizes are used in the experiments (Table 1): (a) Cylindrical probe: The diameter is 0.3 mm, and the exposed area is approximately  $2.9 \text{ mm}^2$ . The probe is mainly used to measure plasma parameters in the near-field area. (b) Ball probe 1: The diameter is 10 mm, and the exposed area is approximately  $465 \text{ mm}^2$ . The probe is mainly used to measure plasma parameters in the mid-field area. (c) Ball probe 2: The diameter is 30 mm, and the exposed area is approximately  $1973 \text{ mm}^2$ . The probe is mainly used to measure plasma parameters in the far field region.

The plasma parameters (plasma potential, density and electron temperature) were measured by the Langmuir probes mounted on the mechanical slide-way. The effective stroke of the slip-way is 900 mm  $\times$  400 mm  $\times$  100 mm. The distribution of the hollow cathode plasma is regarded as rotationally symmetric about its central axis. The whole field measurement can be simplified as the measurement of a plane on one side of the axis. The coordinate system in this paper adopts the cylindrical coordinate system. The measurement grid nodes are

**Table 1**  
Estimation of probe parameters under different plasma densities.

	Plasma density/m <sup>-3</sup>				
	$10^{17}$	$10^{16}$	$10^{15}$	$10^{14}$	$10^{13}$
Debye length/mm	0.013	0.041	0.129	0.407	1.288
The diameter of probes/mm	0.13	0.41	1.29	4.07	12.88

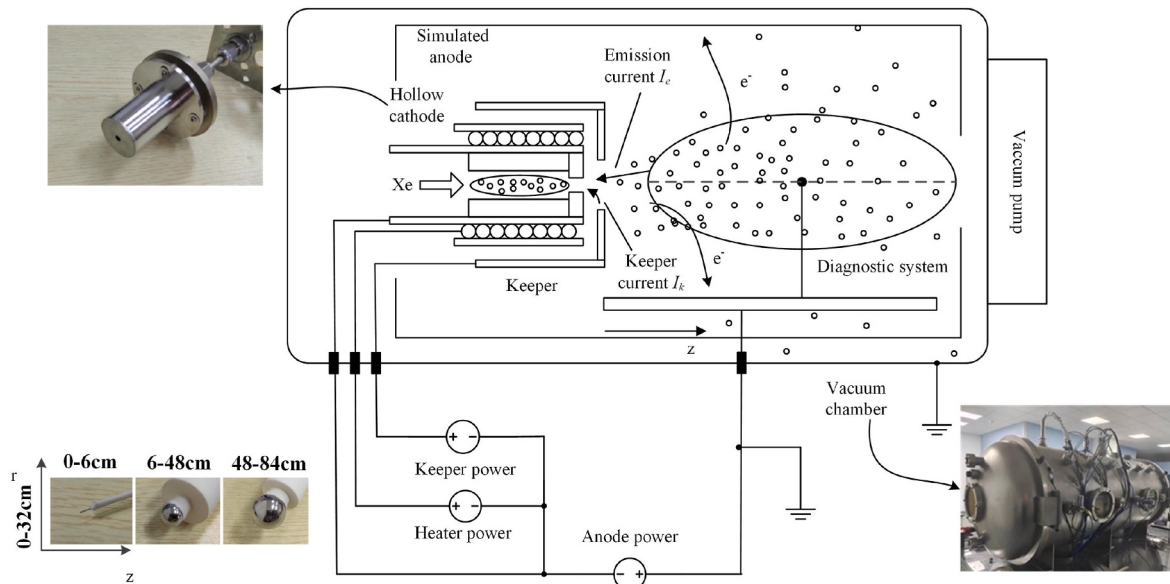


**Fig. 1.** Schematic diagram of the basic scheme of the hollow cathode ground test.

distributed at equal intervals with axial measurement interval of 3 cm and radial measurement interval of 2 cm. The three probes were placed on the slip-way at the same time. When the plasma parameters in different regions (near-field, mid-field and far-field regions) are measured, different probe (Cylindrical probe, Ball probe 1 and Ball probe 2) circuits are connected.

It should be noted that, unlike the previous ground experiment schemes for hollow cathode, in this study a self-made simulated anode (cuboid anode, 80cm × 80cm × 140 cm) is used instead of an actual vacuum chamber, since it is easier to adjust the dimensions of the self-made simulated anode compared with the actual vacuum chamber. Besides that, it is more convenient to clean the simulated anode surface before each ground experiment.

The ground test will measure the following emission current conditions  $I_e$ : 0.001 A, 0.005 A, 0.01 A, 0.02 A, 0.05 A, 0.1 A, 0.2 A, 0.3 A, 0.4 A, 0.5 A, 0.6 A, 0.8 A, 1.0 A, 1.5 A, 2 A, 3 A, 4 A, 5 A. Typical operating conditions are a keeper current  $I_k$  of 2 A, a xenon gas flow rate  $Q$  of 6 sccm, and a distance  $d_k$  of 1.5 mm between the top of the cathode and the keeper.

### 3. Experimental results and discussion

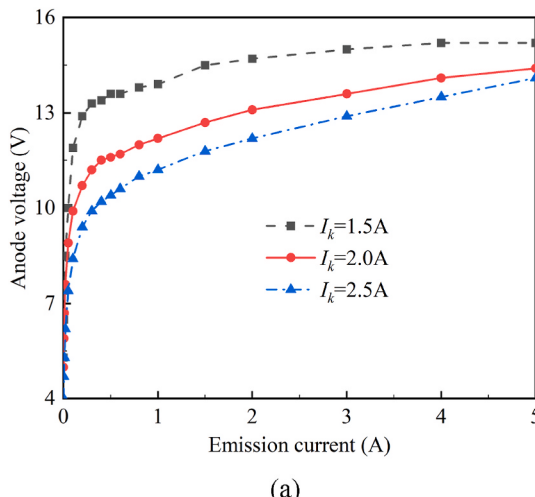
#### 3.1. Effect of keeper current conditions

In this section, the xenon gas flow rate  $Q$  is set at 6 sccm and the distance between keeper and cathode top  $d_k$  is 1.5 mm. This section only changes the current of the keeper ( $I_k = 1.5$  A, 2 A, 2.5 A), and the emission current  $I_e$  varies in the range of 0–5 A.

##### 3.1.1. Comparative analysis of emission characteristics

**Fig. 2 (a)** shows the emission characteristics of hollow cathode under different keeper currents. The anode voltage  $V_a$  reduces with the keeper current from  $I_k = 1.5$  A–2.5 A. The increment of anode voltage slows down with increasing the keeper current, which indicates that the effect of improving the emission characteristics (reducing anode voltage) is gradually weakened with the keeper current. Besides that, the effect of the keeper current  $I_k$  on the anode voltage is more pronounced when the emission current  $I_e$  is relatively small ( $I_e < 1$  A). In this case, the proportion of the keeper current to the total discharge current  $I_d$  (the sum of the keeper current and emission current,  $I_d = I_k + I_e$ ) is relatively high, the emission characteristics of hollow cathode is mainly limited by the keeper current.

In addition, the keeper voltage  $V_k$  monotonically reduces with increasing the emission current in the range of 0–5 A (**Fig. 2 (b)**). The drop amplitudes are approximately 21 V at 1.5 A keeper current, and



(a)

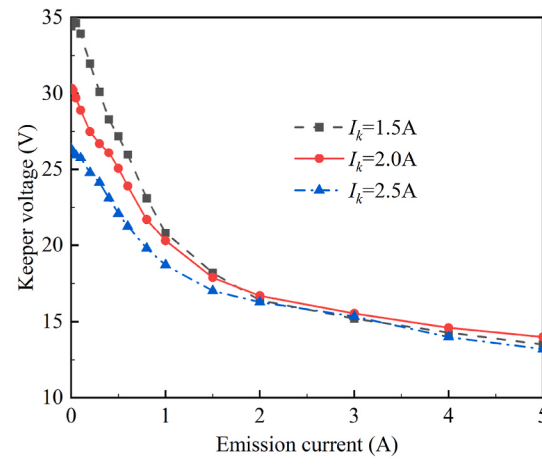
about 12 V at 2.5 A keeper current. This is also related to the ratio of the keeper current to the emission current. The ratio of 1.5 A, 2.0 A and 2.5 A keeper current to the total maximum discharge current (when  $I_e = 5$  A) are about 23.1%, 28.5% and 33%, respectively. When the ratio of keeper current is larger, the working state of the keeper electronic circuit is less likely to be disturbed by the anode electronic circuit.

It should be noted that the changes of the anode voltage and the keeper voltage to the emission current are different: under a given keeper current, the anode voltage generally increases with the emission current when the keeper current is fixed, while the keeper voltage decreases with the increase of the emission current. Although both the keeper electronic circuit and the anode electronic circuit belong to the external flow field of the hollow cathode, the variation rules obtained are obviously different. The coupling region of the two circuits is from the emitter to the cathode top, and the uncoupling region are from the cathode top to the keeper surface and from the cathode top to the anode surface. The characteristics of the former one (cathode top to the keeper surface) are very close to the cathode top outlet, the plasma is not fully expanded, and the working gas density is high. While the latter one (the cathode top to the anode surface) is very far from the cathode top outlet, the plasma is fully expanded, and the working gas density shows a larger magnitude change. When the emission current is larger, the anode needs to absorb the more electrons. Consequently, the plasma density between the cathode top and keeper increases, leading to the decrease of keeper circuit resistance and keeper voltage under a fixed keeper current.

##### 3.1.2. Comparative analysis of plume structure

The effects of the keeper currents on the emission characteristics of hollow cathode will be reflected in the plume structure. **Fig. 3(a)** shows the dependence of plasma potentials at the keeper outlet (0,0) point on the emission current under different keeper currents. The plasma potential at point (0,0) is an important parameter to characterize the performance of the internal flow field of the hollow cathode. The plasma potential at (0,0) reduces with the keeper current, which indicates that the emission characteristics in the internal flow field are improved. When the keeper current is relatively low ( $I_k < 2.0$  A), the plasma potential decreases with the emission current. While when the keeper current reaches to 2.5 A, the plasma potential increases with the emission current, indicating that the discharge behavior in the internal flow field has been significantly affected by the keeper current.

To further evaluate the contribution of the keeper current on the discharge characteristics of internal and external flow fields, the changes of plasma potential at point (0,0)  $\Delta V_{in}$  ( $V_{(0,0)}(I_k = 1.5\text{A}, 2.5\text{A}) - V_{(0,0)}(I_k = 2.0\text{A})$ ) and anode voltage  $\Delta V_a$  ( $V_a(I_k = 1.5\text{A}, 2.5\text{A}) - V_a(I_k = 2.0\text{A})$ ) are firstly calculated. After that, the difference between



(b)

**Fig. 2.** The effects of keeper currents on (a) emission characteristics and (b) keeper characteristics.

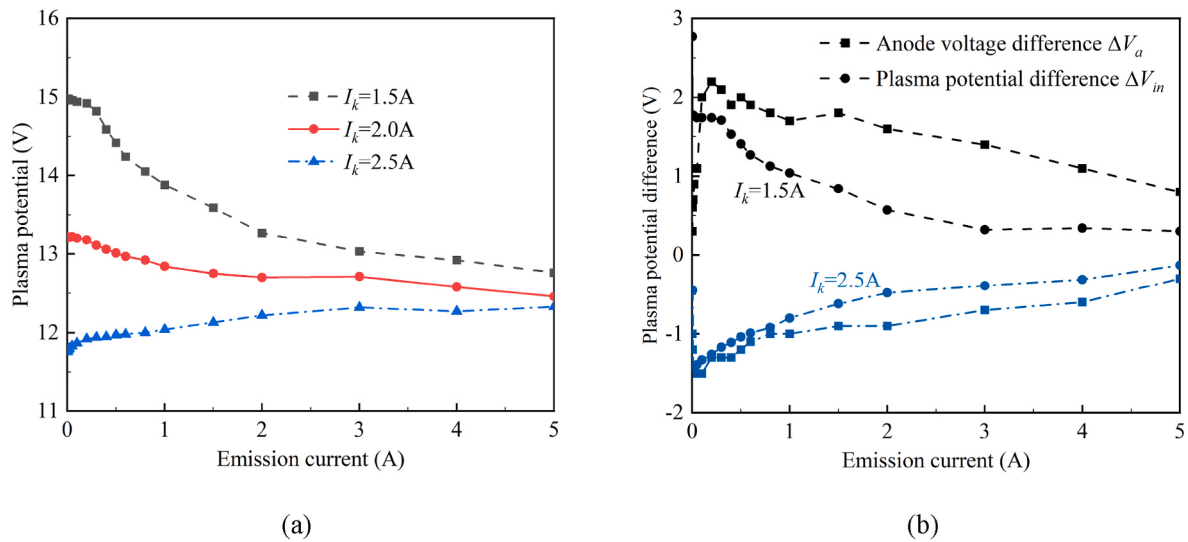


**Fig. 3.** The effects of keeper currents on (a) plasma potential at (0,0) position and (b) anode voltage variation and plasma potential difference change of internal flow field.

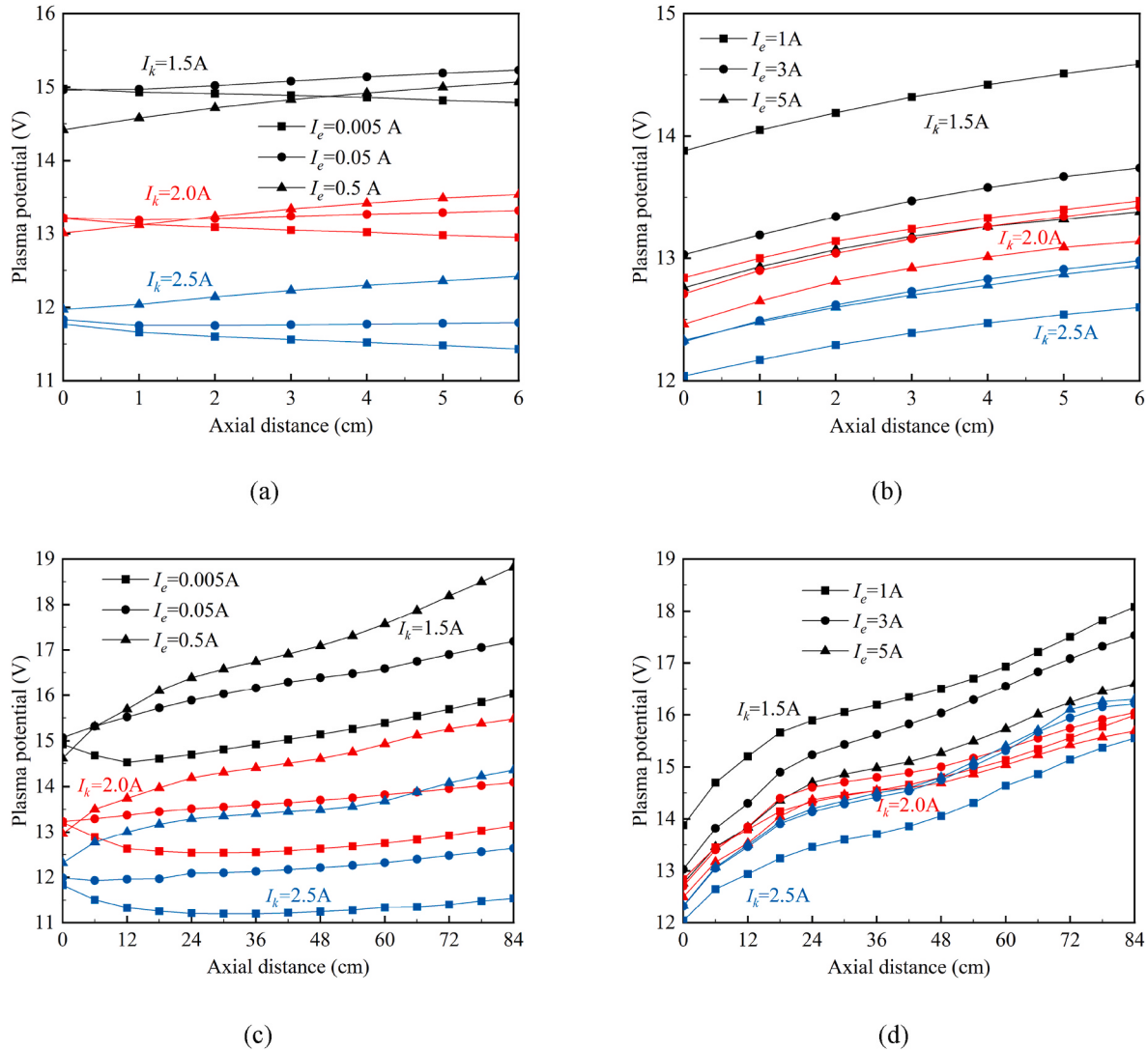


**Fig. 4.** The effects of keeper currents on plasma potential in the near-field area: (a) low emission currents, (b) high emission currents; and in the far-field area: (c) low emission currents, (d) high emission currents.

$\Delta V_a$  and  $\Delta V_{in}$  ( $\Delta V_{ex} = \Delta V_a - \Delta V_{in}$ ) is used to further characterize the performance of the discharge characteristics of external flow field of the hollow cathode. When the emission current is low ( $I_e < 0.5$  A), the plasma potential difference of the external flow field  $\Delta V_{ex}$  is far less than that of the internal flow field  $\Delta V_{in}$ , which indicates that the change of the plasma potential of the internal flow field is the main reason for the change of the anode voltage, and the discharge characteristics of the external flow field is not significantly affected at this time. While with the increase of emission current ( $I_e \geq 0.5$  A), the change of internal plasma potential and external plasma potential all leads to the change of anode voltage. At this time, the external flow field will also be changed.

In order to evaluate the effect of keeper current on the plume structure, the axial distributions of plasma potential under different keeper currents have been given (Fig. 4). Due to the large number of data points, only part of the data has been given. Among them, the measurement intervals in the near-field area (0–6 cm) and far-field area (6–84 cm) is 1 cm and 6 cm, respectively. When the plasma potential at (0,0) is the smallest in the near-field area, the plume structure is considered “positive potential plume”; when the plasma potential at (0,0) is the largest in the near-field area, the plume structure is referred to “negative potential plume” [23,24]. As can be seen that, when the keeper current is 1.5 A, the transitions of the plume structure from “positive potential plume” to “negative potential plume” occur when the emission current reaches to 0.02–0.05 A, while when the keeper current is above 2.5 A, the transitions of plume structure happens around  $I_e = 0.05$  A. Therefore, the keeper current does not have a significant influence on the transition conditions between those two different plume structures.

Note that, under relative low emission current ( $I_e < 0.5$  A), the effect of the keeper current on the plasma potential is more pronounced compared with that under high emission current ( $I_e > 1$  A). Due to the transition of plasma structure in the low emission current, the difference of plasma potential by axis ( $U_{(48,0)} - U_{(0,0)}$ ) increases with the emission current, while this difference almost unchanged in the high emission current regions (1 A–5 A). It is interesting to find that, the plasma potential at a given point in the far-field (>6 cm) does not always rise up with increasing the emission current. For example, under  $I_k = 1.5$  A, the plasma potential at the point (48 cm, 0 cm) firstly rises up with the emission current, after that it start to decreases under a further increase of the emission current. The transition point  $I_{e,tr}$  corresponding to the maximum plasma potential depends on the keeper current, it shifts from  $I_{e,tr} = 0.5$  A to  $I_{e,tr} = 3$  A when the keeper current is 1.5 A and 2.0 A, respectively. Since the effect of keeper current on axial plasma potential could be neglected under very high emission current  $I_e > 5$  A, the transition point of emission current is absent when the keeper current is 2.5 A. In this case, the plasma potential at a given point in the far field region monotonically rises up with the emission current. This diagram is of substantial importance for selecting an optimal working conditions to guarantee the minimum anode potential (improve emission characteristics).

The effect of keeper current on the two-dimensional plasma potential distribution at 1 A emission current is shown in Fig. 5. The plasma potential distribution has certain similarity: the contour distribution shape in the near-field region (0–6 cm in the axial direction, 0–8 cm in the radial direction) is basically the same; There is a slight difference in the plasma potential distribution of the middle-field area and the far-field area, especially under 2.5 A keeper current, the angle between contour of plasma potential and axis is more vertical than the other two working conditions. Therefore, when the keeper current is lower, the plume deflection effect [25] of hollow cathode is more pronounced and the deflection angle  $\theta$  of hollow cathode plume structure is smaller. The plume deflection angle of hollow cathode is directly connected with the spatial equivalent resistance, which is of substantial importance for the Hall and ion thrusters when the hollow cathode serves as a neutralizer. The interaction effect of ion beam from the ion thruster with the electrons from the hollow cathode and the equivalent circuit between them

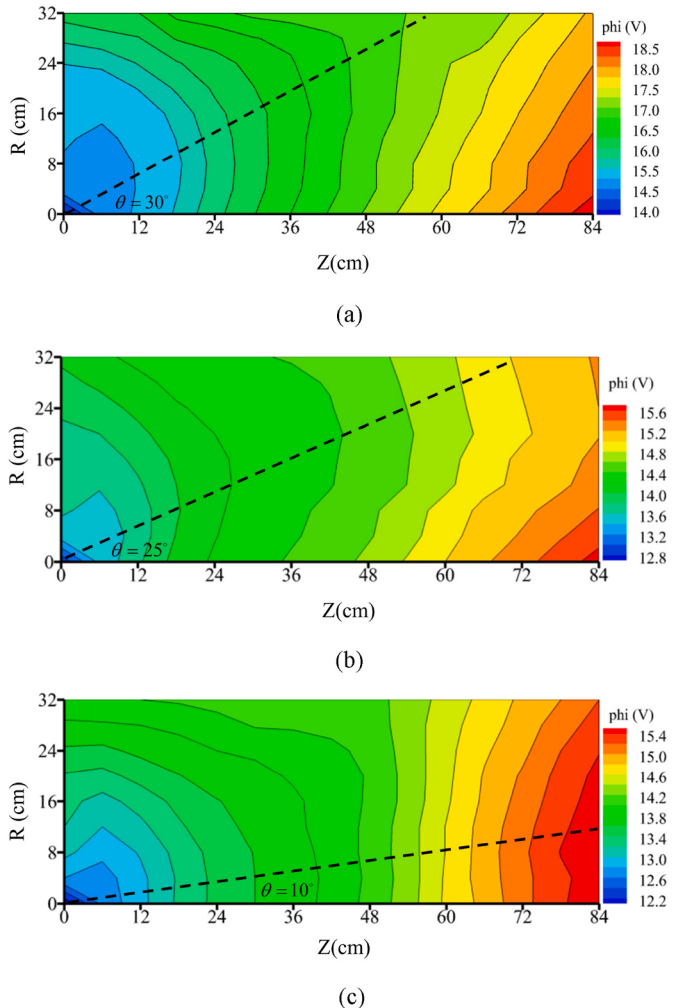
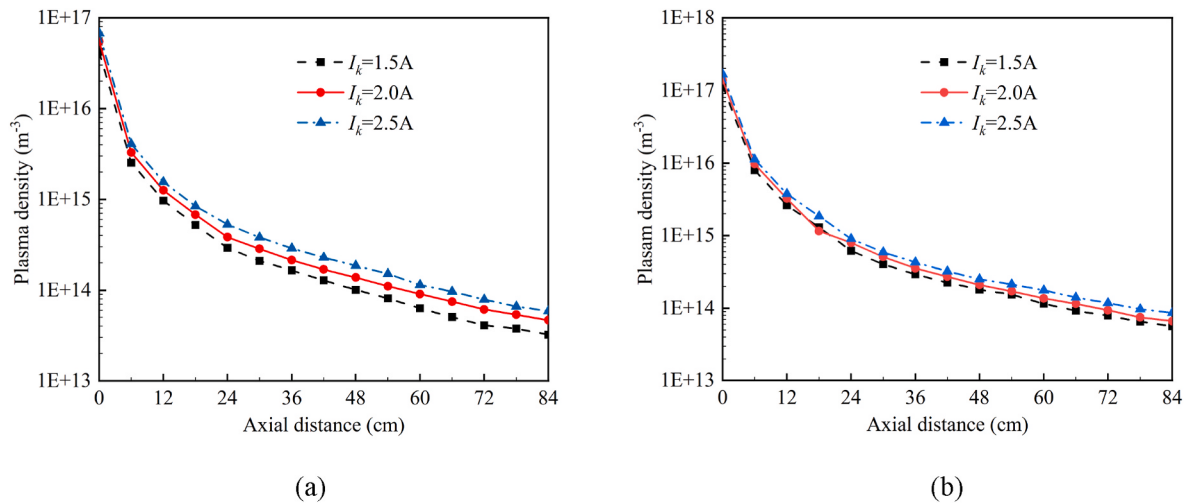


Fig. 5. Comparison of two-dimensional plasma potential distribution under  $I_e = 1$  A emission current and different keeper currents (a)1.5 A (b)2.0 A (c) 2.5 A.

will significantly changes with the enlarge of the plume deflection angle of hollow cathode. Therefore, a systematical study of the effect of working conditions on the plume deflection angle should be made. The experimental results show that when keeper current is larger, the plasma diffusion of hollow cathode is more focused, and the discharge performance is better.

The drops of plasma density in the plume structure mainly happens in the near-field region (from  $1 \times 10^{17}$  to  $5 \times 10^{15} \sim 1 \times 10^{16} \text{ m}^{-3}$ ). While in the far-field regions the plasma diffusion process slows down (Fig. 6). By comparing the axial distribution of plasma density under low and high emission current, it can be seen that, the increases of the emission current from 0.5 A to 5 A (in 10 times) only leads an increase of the plasma density in 2–3 times, the increment ratio of plasma density at a given point isn't proportional to the increment ratio of the emission current.

The effect of the keeper current on the plasma density is more pronounced under a relatively small emission current ( $I_e = 0.5$  A) (Fig. 6 (a)). As can be seen that, when the emission current is  $I_e = 0.5$  A, the plasma density rises up about 21% with the increase of the keeper current from 1.5 A to 2.5 A, while under a relative high emission current  $I_e = 5$  A, the axial distribution of plasma density only rises up about 6% with increasing the keeper current from 1.5 to 2.5 A. The reason for this phenomenon is the same as that mentioned before. The higher the emission current, the smaller effect of the keeper current on the working performance of the hollow cathode. In this section, the xenon gas flow



**Fig. 6.** The effects of keeper currents on plasma density under different emission currents (a)  $I_e = 0.5$  A (b)  $I_e = 5$  A 3.2 Effect of distance between keeper and cathode top.

rate is set at 6 sccm and the keeper current is 2 A. This section only changes the distances between keeper and cathode top ( $d_k = 1.5$  mm,  $2.5$  mm), and the emission current also varies in the range of 0–5 A.

A schematic diagram of the characteristics of the keeper electronic circuit is shown in Fig. 7. When the keeper is close to the cathode top ( $d_k = 1.5$  mm), the absorbing surface of electrons by the keeper is mainly through its inner wall. In this case, the limitation of keeper structure on the outward expansion of the plasma plume is relatively small. When  $d_k$  is larger, the surface of the keeper absorbing electrons also includes the keeper bottom surface. In this case, a significant obstacle may form to hinder the outward movement of plasma particles.

### 3.1.3. Comparative analysis of emission characteristics

Fig. 8(a) shows the emission characteristics of hollow cathode under  $d_k = 1.5$  mm and  $2.5$  mm. The emission characteristic curves are completely different. Only when the emission current is smaller than 0.1 A, the effect of the keeper distance  $d_k$  on the anode voltage and keeper voltage could be neglected. While under a relatively high emission current ( $I_e > 0.2$  A), the values of anode voltage and keeper voltage could be almost in 1.5–2 times higher when the distance between keeper and cathode top extend from  $d_k = 1.5$  mm– $2.5$  mm. This may be due to the fact that when the  $d_k$  is large enough, the keeper forms a significant obstacle to the discharge of the anode and keeper electronic circuit, this obstacle not only causes an increase in the anode voltage and keeper voltage, but also leads to the discharge instability of hollow cathode. The detailed discussion about the effect of keeper distance  $d_k$  on discharge instability would be detailed discussed in Section 3.3.

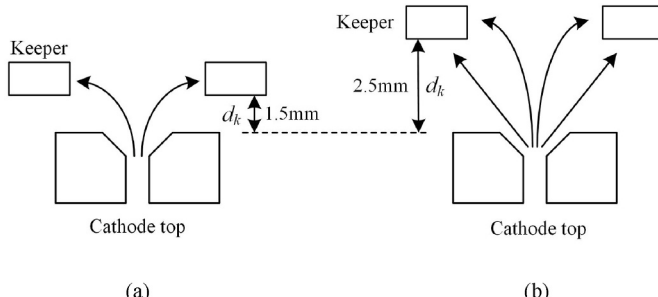


**Fig. 7.** The effect of keeper on the plume of hollow cathode at different distances between keeper and cathode top  $d_k$ : (a)  $d_k = 1.5$  mm; (b)  $d_k = 2.5$  mm.

### 3.1.4. Comparative analysis of plume structure

In order to study the effect of  $d_k$  on the plume structure of hollow cathode, the emission current is set at 1 A. Fig. 9 shows the axial and radial plasma potential distributions under different  $d_k$ . The plasma potential at the initial measurement point (0,0) of  $d_k = 1.5$  mm and  $d_k = 2.5$  mm is 12.84 V and 12.51 V, respectively. Considering the measurement errors of the Langmuir probes, it can be considered that  $d_k$  does not affect the discharge condition in the region from the emitter to the initial measurement point (0,0) under the typical working condition. The effect of the distance between keeper and cathode top on the plasma plume structure could be divided into two separated regions. In the near-field region (0–6 cm), the plasma potential distribution curves almost coincide at different  $d_k$ , the effect  $d_k$  of on the internal field can be ignored. In the middle- and far-field region, the axial and radial plasma potentials are greater when  $d_k = 1.5$  mm, the plasma potential difference between  $d_k = 1.5$  mm and  $d_k = 2.5$  mm is kept at about 1 V in the axial direction, and is slightly smaller in the radial direction at about 0.4–0.6 V.

The radial potential decay rate at  $d_k = 2.5$  mm is larger than  $d_k = 1.5$  mm, which indicates that the radial diffusion of plasma plume is hampered at  $d_k = 2.5$  mm (Fig. 10). The plasma potential at (0,0) is still the minimum value (about 13.0 V) and the plasma potential on the central axis (84,0) is still the maximum value (about 16.5 V). The deflection angle is increased by 10° at  $d_k = 2.5$  mm compared to  $d_k = 1.5$  mm. The experimental results show that  $d_k$  will worsen the discharge performance of hollow cathode.

The distance between the keeper outlet and the cathode top has little effect on the distributions of axial and radial plasma density of the plume (Fig. 11). The plasma density still reduces quickly along axis in the near-field region, the decay rate gradually decreases with the increasing of axial or radial distance, and the decay rate in the radial direction is greater than that in the axial direction. When  $d_k = 1.5$  mm and  $2.5$  mm, the plasma density at the initial measurement point (0,0) is  $7.25 \times 10^{16} \text{ m}^{-3}$  and  $7.01 \times 10^{16} \text{ m}^{-3}$  respectively. Considering the measurement and data processing errors, it can be considered that there is basically no change at different  $d_k$ , which means that the internal field (the emitter to the keeper outlet) of hollow cathode is almost not affected by  $d_k$ .

### 3.2. Discharge stability analysis

Fig. 12 shows the discharge images of the hollow cathode plume ( $I_k = 2$  A,  $Q = 6$  sccm) under different emission current conditions. For the hollow cathode, the external plume structure is mainly related to the de-excitation of neutral atoms and ions [26]. The high-energy electrons

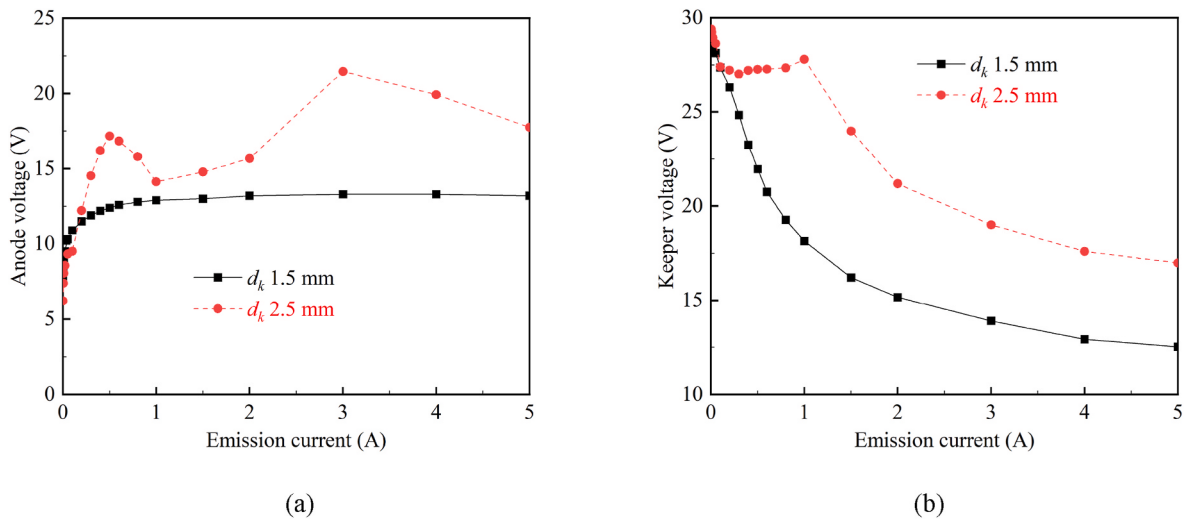


**Fig. 8.** The effects of different distances between the keeper and cathode top on (a) emission characteristics and (b) keeper characteristics.

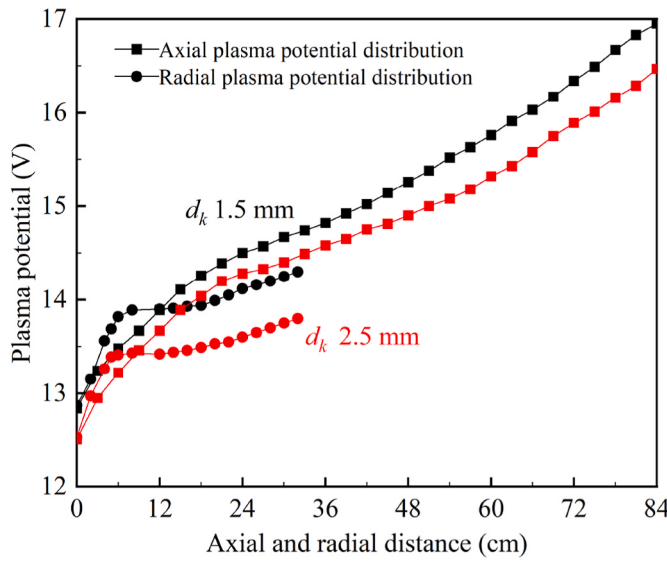


**Fig. 9.** Comparison of axial and radial plasma potential distribution.

collide with these particles to put them in an unstable excited state, and the electrons in the outer orbit of the excited particle jump to the inner orbit to emit photons, so as to produce light of specific wavelength. In general, when the number of high-energy electrons in the plume is higher, the luminous intensity and area are greater, which is particularly evident in the “plume mode” of hollow cathode [19].

When the emission current is small ( $I_e < 1 \text{ A}$ ), only the outlet of the keeper shows obvious bright light. At this time, most particle collisions only occur in the emission to the keeper of the hollow cathode, the emission current  $I_e$  and anode voltage  $V_a$  are small, and the collision probability of the external plume area is low, so there is no obvious luminous area. With the continuous increase in the emission current ( $I_e \geq 1 \text{ A}$ ), the luminous intensity and area increase significantly with the emission current in the external plume. This kind of more diffuse plasma is associated with the “plume mode” of the hollow cathode [27, 28], and the hollow cathode discharge begins to be unstable in the “plume mode”, which is consistent with the previous literature [29,30].

The change in the emission current  $I_e$  with time when  $d_k = 1.5 \text{ mm}$ ,  $I_k = 2 \text{ A}$  is given in Fig. 13. The y-axis in Fig. 13 corresponds to the oscillation amplitude of emission current. As shown in Fig. 13, the oscillation amplitude of hollow cathode discharge parameters is small,

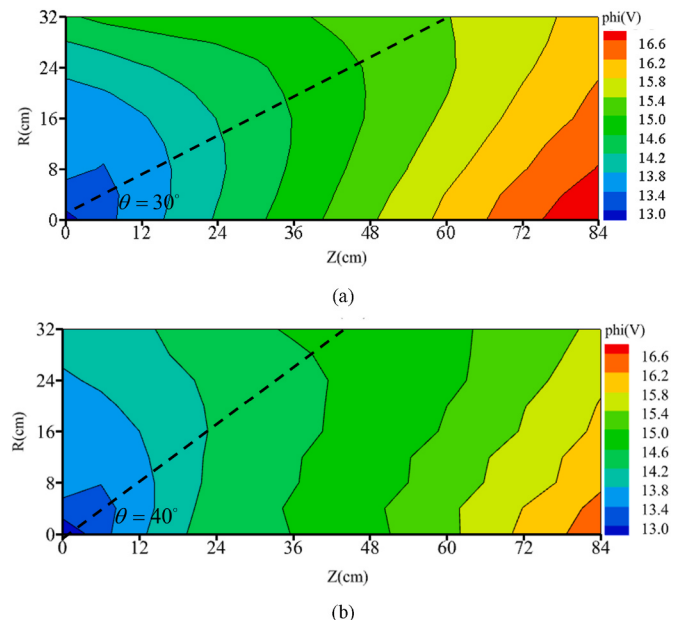


**Fig. 10.** Comparison of two-dimensional plasma potential distribution under different distances between keeper and cathode top (a) 1.5 mm; (b) 2.5 mm.

the hollow cathode discharge could be considered stable under all emission current conditions. Moreover, the amplitude of the discharge oscillation increases with the emission current, which is consistent with the change in the discharge image observed in Fig. 12.

The excessive  $d_k$  will lead to a more intensive discharge instability of hollow cathode, the anode voltage will increase and the performance and lifetime of hollow cathode may significantly become worsen. Fig. 14 shows the change of emission current  $I_e$  with time when  $d_k = 2.5 \text{ mm}$ . As can be seen that, the oscillation amplitude of emission current is larger compared with that under  $d_k = 1.5 \text{ mm}$  in all emission current cases ( $I_e = 0.005\text{--}5 \text{ A}$ ). The emission current waveform characteristics can be approximated as a “triangular wave” or “saw-tooth wave”. The basic oscillating waveform of the emission current is composed of two waveforms with different characteristics: a positive large-amplitude low-frequency wave and a negative small-amplitude high-frequency wave. From the emission current oscillation waveform, the positive amplitude of the low-frequency wave is much larger than the negative amplitude of the high-frequency wave (this can be explained by the

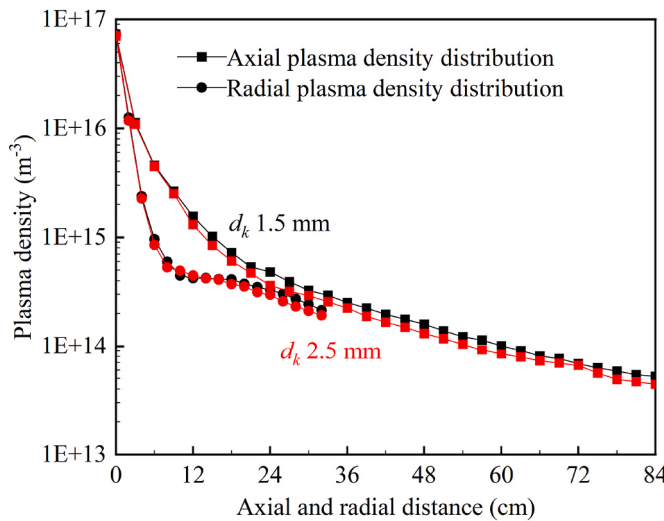


Fig. 11. Comparison of axial and radial plasma density distribution.

emission characteristic curve [31]). Moreover, the amplitude of discharge oscillation increases with the emission current, which is the same as the change rule when  $d_k = 1.5$  mm.

Fast Fourier analysis was performed on the emission current waveform under  $d_k = 2.5$  mm, and its amplitude-frequency analysis is shown in Fig. 15. For all listed emission current conditions, the low frequency corresponding to the main oscillation amplitude is below 10 kHz, and the frequency decreases gradually with increasing emission current. While when the emission current is relatively small ( $I_e = 0.005$  A and 0.05 A), an obvious oscillation amplitude at approximately 200 kHz could be observed. The significant different magnitude of oscillation frequencies indicates that the mechanism of oscillation generation is different. The range of xenon ionization frequency is generally below

100 kHz [19], so the low oscillation frequency corresponding to the main amplitude (<10 kHz) is caused by ionization instability, and the emission current pulse corresponds to the ionization aggregation and dissipation of xenon ions in space.

The high-frequency oscillations within oscillation frequency around 200 kHz is connected with the ion acoustic turbulence [32,33]. Usually the excitation frequency  $\omega$  range of ion acoustic waves is greater than the collision frequency of the ion and neutral gas  $\nu_{in}$  and less than the plasma frequency  $\omega_{pi}$ :

$$\nu_{in} < \omega < \omega_{pi} \quad (1)$$

The collision frequency of the ion and neutral gas  $\nu_{in}$  can be expressed as [34]:

$$\nu_{in} = n_n \sigma_{CEX} V_i \quad (2)$$

where,  $n_n$  is the density of neutral gas,  $\sigma_{CEX}$  is the charge exchange cross section, and  $V_i$  is the ion velocity. The density of neutral gas  $n_n$  at the hollow cathode outlet is approximately  $10^{20} \text{ m}^{-3}$  [35]. The charge exchange-cross section  $\sigma_{CEX}$  is  $1 \times 10^{-18} \text{ m}^{-2}$  [18], the ion velocity  $V_i$  is approximately 2 km/s [25,32]. Therefore, the collision frequency of ion and neutral gas  $\nu_{in}$  is approximately 180 kHz. The plasma frequency can be expressed as:

$$\omega_{pi} = \sqrt{n_i |e|^2 / (\epsilon_0 m_i)} \quad (3)$$

where,  $n_i$  is the ion density,  $e$  is the elementary charge,  $\epsilon_0$  is the vacuum dielectric constant and  $m_i$  is the xenon ion mass. The ion density  $n_i$  at the cathode outlet is approximately  $10^{17} \text{ m}^{-3}$  (Fig. 15), and the plasma frequency  $\omega_{pi}$  is approximately 100 MHz. Therefore, the excitation frequency range of ion acoustic wave  $\omega$  generally starts from 180 kHz and is less than 100 MHz. In this experiment, the high frequency of emission current pulse oscillation (approximately 200 kHz) is within its range according to the fast Fourier analysis.

Since the extend of  $d_k$  will lead to an extreme discharge instability of

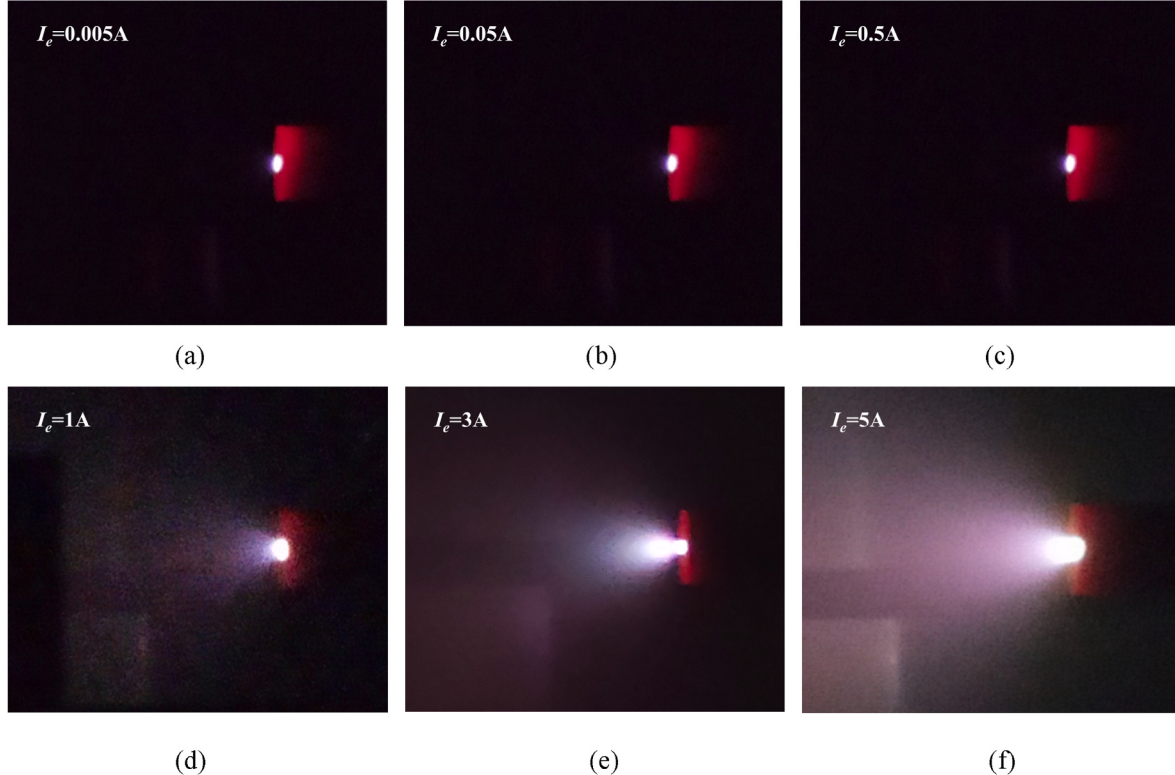
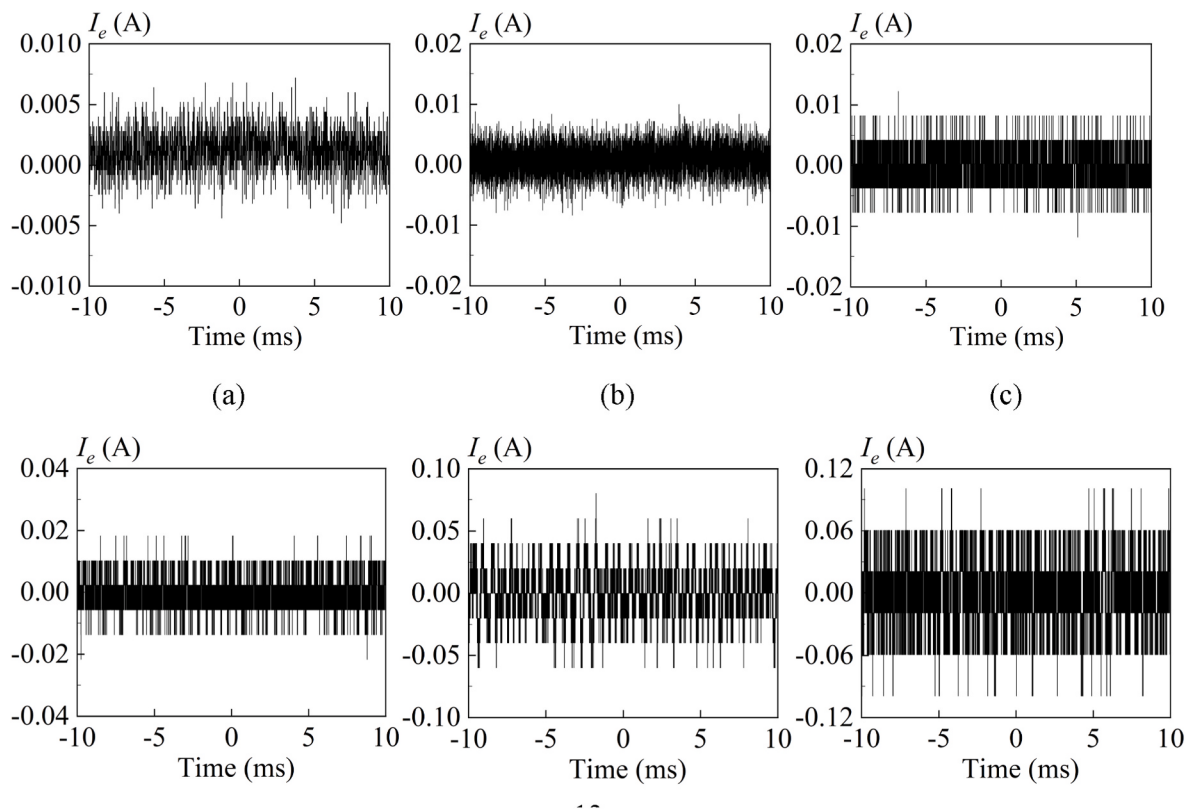
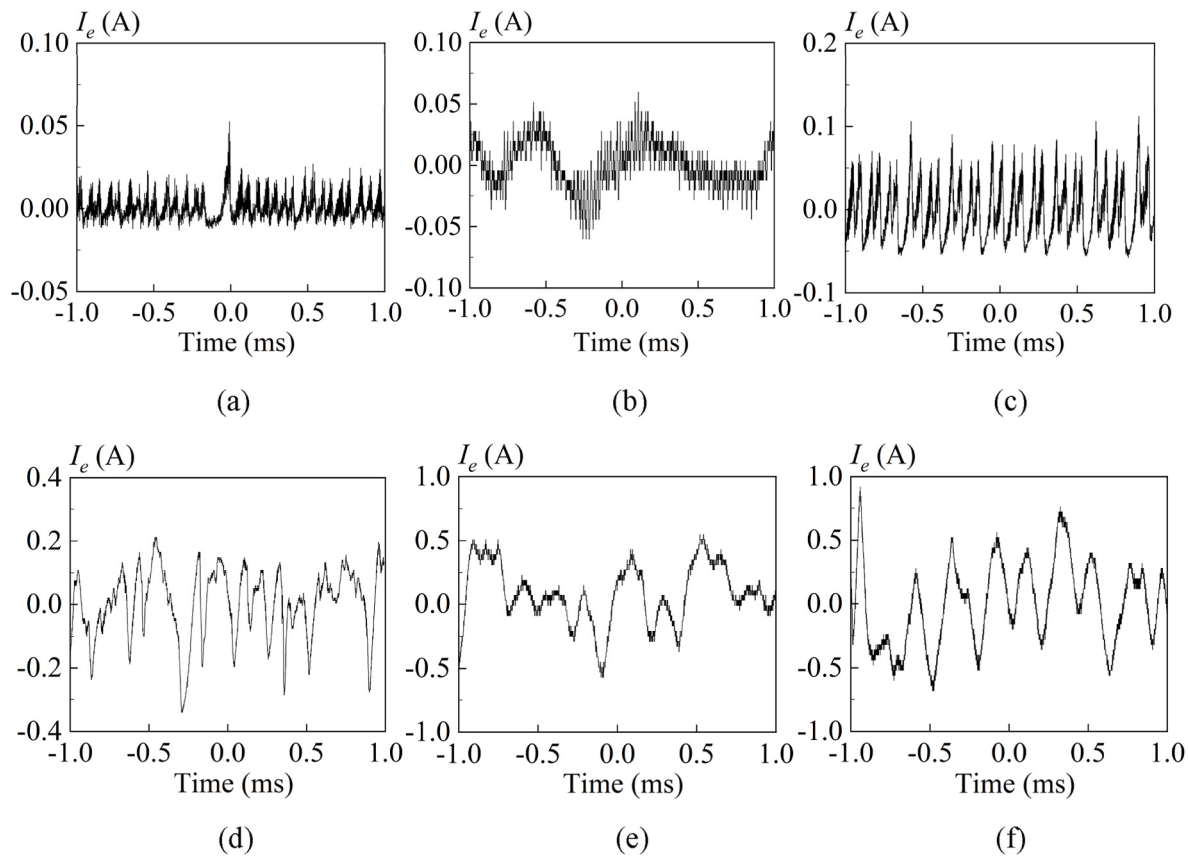


Fig. 12. Discharge images of hollow cathode plume under different emission currents (a) 0.005 A, (b) 0.05 A, (c) 0.5 A, (d) 1 A, (e) 3 A, (f) 5 A



**Fig. 13.** Stability analysis of hollow cathode under different emission currents: (a) 0.005 A, (b) 0.05 A, (c) 0.5 A, (d) 1 A, (e) 3 A, (f) 5 A when  $d_k = 1.5 \text{ mm}$ .



**Fig. 14.** Stability analysis of hollow cathode under different emission currents: (a) 0.005 A, (b) 0.05 A, (c) 0.5 A, (d) 1 A, (e) 3 A, (f) 5 A when  $d_k = 2.5 \text{ mm}$ .

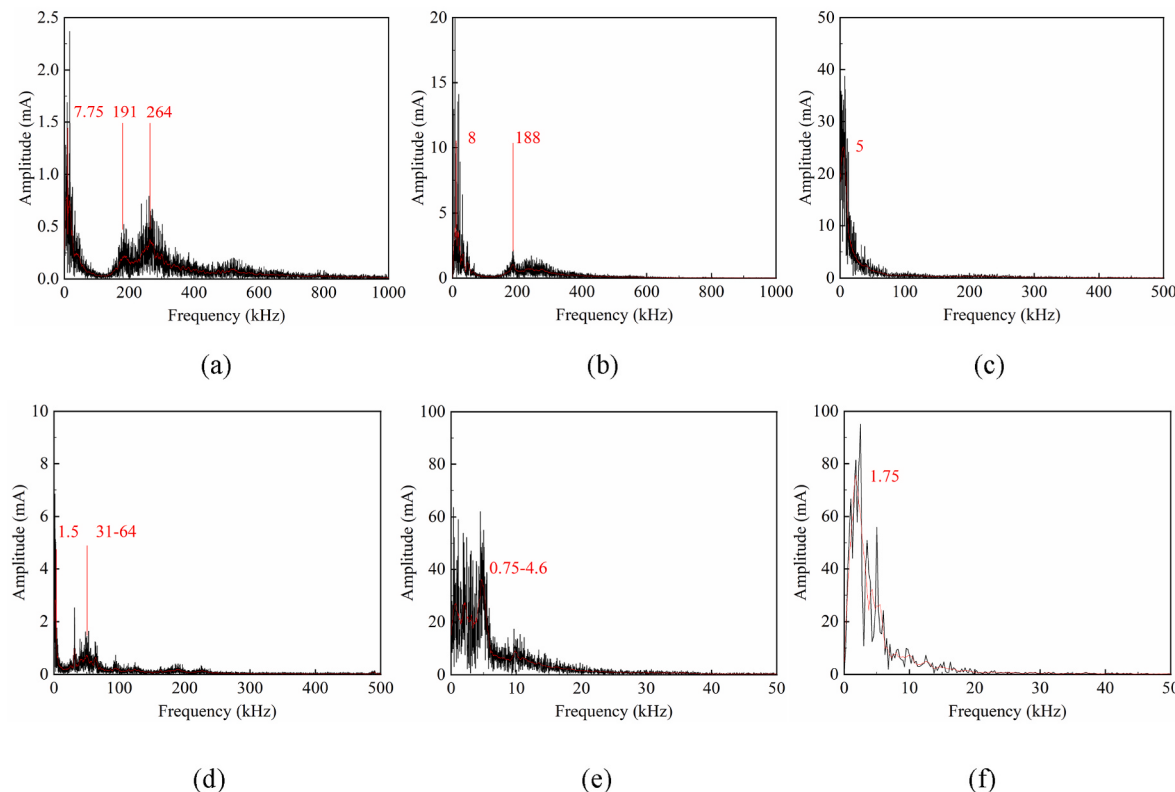


**Fig. 15.** Fast Fourier analysis of different emission currents: (a) 0.005 A (b) 0.05 A (c) 0.5 A (d) 1 A (e) 3 A (f) 5 A.

the hollow cathode. To obtain a stable discharge state the xenon gas flow rate should be adjusted [31]. In this work the dependence of the unstable discharge characteristics of hollow cathode on the xenon gas flow rate, emission current and keeper currents is studied when  $d_k = 2.5$  mm. Around the typical operating conditions ( $Q = 6$  sccm,  $I_k = 2.0$  A), a series of working conditions were carried out (Table 2).

Fig. 16 shows the emission characteristics and oscillation characteristics of the hollow cathode under different xenon flow rates and keeper currents, where the relative oscillation amplitude of emission current on y-axis of Fig. 16 (b) is defined as:  $(I_{e,peak} - I_e)/I_e$ . Under F6K20, F6K15, and F4K20 operating conditions, significant discharge instability occurs, and the relative oscillation amplitudes of F6K15, and F4K20 are greater than amplitude of F6K20, which indicates that hollow cathode discharge under lower xenon gas flows and keeper currents are more likely to provoke discharge instability; With the increase of keeper current to  $I_k = 2.5$  A, the relative oscillation amplitude is only above 0.1 under small emission current  $I_e = 1.0$  A. Besides that, the relative oscillation amplitude of emission current is always less than 0.1 for F8K20 case, which can also be considered as basically non-oscillational. As a result, the stable operation boundary of hollow cathode becomes smaller with the increase of  $d_k$ : a higher xenon flow rate  $Q$  and greater keeper current  $I_k$  are required to achieve the stable working state of hollow cathode under all emission current  $I_e$ .

#### 4. Conclusion

A series of ground experiments were performed to investigate the influence of keeper working conditions on the discharge characteristics of hollow cathodes. The effects of the keeper current and the distance between the keeper and cathode top on the emission characteristics and plume structure of the hollow cathode were determined. Moreover, the discharge stability of hollow cathode under different keeper working conditions was analyzed. The ground experiment results provide useful information for instructing hollow cathode design and working condition selection.

- The effect of the keeper current on the emission characteristics and plume structure of the hollow cathode mainly depends on its ratio to the emission current ( $I_k/I_e$ ). When the proportion of keeper current is large, the working state of the keeper electronic circuit is less likely to be disturbed by the anode electronic circuit, and it has a greater impact on the emission characteristics and plume structure. The plasma potential on the emission current does not always rise up with the emission current in the far-field ( $>6$  cm) when the keeper current is not high ( $<3$  A). The transition point  $I_{e,tr}$  corresponding to the maximum plasma potential depends on the keeper current, it shifts from  $I_{e,tr} = 0.5$  A to  $I_{e,tr} = 3$  A when the keeper current is 1.5 A and 2.0 A, respectively.
- The distance between the keeper and cathode top  $d_k$  also has a significant impact on the working performance of the hollow cathode. When  $d_k$  is large enough, the keeper forms a significant obstacle to the discharge of the anode electronic circuit, this obstacle causes an increase in the anode voltage and emission characteristics of hollow cathode are worse. The effect of  $d_k$  on the plasma potential distribution is more pronounced in the far-field region. When  $d_k = 1.5$  mm, the axial and radial plasma potential is greater than  $d_k = 2.5$  mm, the plasma potential difference between  $d_k = 1.5$  mm and  $d_k = 2.5$  mm is kept at about 1

**Table 2**  
Ground experiment controllable conditions.

Keeper current $I_k$ /A	Xenon flow rate $Q$ /sccm		
	4	6	8
1.5	×	F6K15	×
2.0	F4K20	F6K20	F8K20
2.5	×	F6K25	×

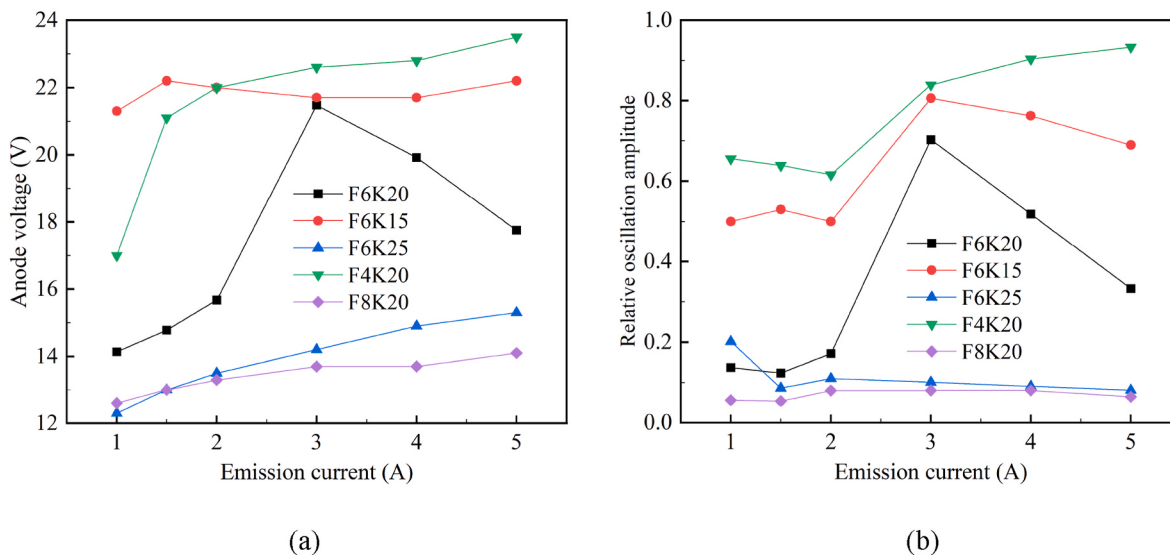


Fig. 16. The (a) emission characteristics and (b) oscillation characteristics of the hollow cathode.

V in the axial direction, and is slightly smaller in the radial direction at about 0.4–0.6 V.

- (iii) The excessive  $d_k$  makes the hollow cathode discharge unstable during operation, which affects not only the increase in anode voltage but also the life and performance of the hollow cathode. The characteristics of emission current oscillation are relatively obvious, and its waveform characteristics can be approximated as a “triangular wave” or “sawtooth wave”. It can be seen from the fast Fourier analysis that the discharge oscillation mainly consists of ionization oscillation of low frequency (<10 kHz) and ion acoustic wave oscillation of high frequency (approximately 200 kHz). The excessive  $d_k$  changes the stable working boundary of the hollow cathode: a higher xenon flow rate  $Q$  and greater keeper current  $I_k$  are required to achieve the stable working state of hollow cathode under all emission current  $I_e$ .

#### Funding sources

This work was supported by the National Natural Science Foundation of China [grant numbers U22B20120, NSFC52177128, NSFC52202460], the National Key R&D Program of China [grant numbers 2020YFC2201100, 2021YFC2202804, 2022YFB3403504], the China Postdoctoral Science Foundation [grant numbers 2021M690392, 2021TQ0036], the Science Foundation for Youth Scholars of Beijing Institute of Technology, and the Advanced Space Propulsion Laboratory of BICE and Beijing Engineering Research Center of Efficient and Green Aerospace Propulsion Technology [grant number LabASP-2021-04].

#### Declaration of competing interest

The authors declare that they have no known competing financial interests or personal relationships that could have appeared to influence the work reported in this paper.

#### References

- [1] T. Takahashi, K. Kinoshita, Low power arcjet thruster using LaB6 hollow cathode, *Acta Astronaut.* 206 (2023) 89–99, <https://doi.org/10.1016/j.actaastro.2023.02.015>.
- [2] R.W. Conversano, G. Beccati, D.M. Goebel, V.H. Chaplin, Demonstration of 13,011 h of operation of a proto-flight compact heaterless lanthanum hexaboride hollow cathode, *Acta Astronaut.* 197 (2022) 53–59, <https://doi.org/10.1016/j.actaastro.2022.05.015>.
- [3] A. Remigy, X. Aubert, S. Prasanna, K. Gazeli, L. Invernizzi, G. Lombardi, C. Lazzaroni, Absolute N-atom density measurement in an Ar/N2 micro-hollow cathode discharge jet by means of ns-two-photon absorption laser-induced fluorescence, *Phys. Plasmas* 29 (2022), 113508, <https://doi.org/10.1063/5.0110318>.
- [4] C.J. Wordingham, P.-Y.C.R. Taunay, E.Y. Choueiri, The attachment length in orificed hollow cathodes, *Plasma Sources Sci. Technol.* 31 (2022), 025018, <https://doi.org/10.1088/1361-6595/ac3d3f>.
- [5] F. Tian, L. Miao, Q. Xia, N. Wang, X. Hou, Analysis of effect of ground experiment environment on plasma contactor performance, *AIAA J.* 61 (2023) 1168–1180, <https://doi.org/10.2514/1.J062310>.
- [6] Y.D. Korolev, N.N. Koval, Low-pressure discharges with hollow cathode and hollow anode and their applications, *J. Phys. D Appl. Phys.* 51 (2018), 323001, <https://doi.org/10.1088/1361-6463/aacf10>.
- [7] G. Sánchez-Arriaga, G. Borderes-Motta, L. Chiabó, A code for the analysis of missions with electrodynamic tethers, *Acta Astronaut.* 198 (2022) 471–481, <https://doi.org/10.1016/j.actaastro.2022.06.021>.
- [8] L. Felicetti, G.B. Palmerini, Three spacecraft formation control by means of electrostatic forces, *Aero. Sci. Technol.* 48 (2016) 261–271, <https://doi.org/10.1016/j.ast.2015.11.022>.
- [9] J.M. Tejeda, A. Knoll, An oxygen-fuelled Hall Effect Thruster: channel length, ceramic walls and anode material experimental analyses, *Acta Astronaut.* 203 (2023) 268–279, <https://doi.org/10.1016/j.actaastro.2022.11.055>.
- [10] T.D. Munro-O'Brien, C.N. Ryan, Performance of a low power Hall effect thruster with several gaseous propellants, *Acta Astronaut.* 206 (2023) 257–273, <https://doi.org/10.1016/j.actaastro.2023.01.033>.
- [11] F. Tian, K. Xie, L. Miao, F. Liang, J. Song, S. Bai, N. Wang, An equivalent model of discharge instability in the discharge chamber of Kaufman ion thruster, *Plasma Sci. Technol.* 24 (2022), 115505, <https://doi.org/10.1088/2058-6272/ac78cb>.
- [12] M. Lee, D. Kim, J. Lee, Y. Kim, M. Yi, A data-driven approach for analyzing Hall thruster discharge instability leading to plasma blowoff, *Acta Astronaut.* 206 (2023) 1–8, <https://doi.org/10.1016/j.actaastro.2023.02.017>.
- [13] M.T. Domonkos, J.E. Foster, G.C. Soulas, Wear testing and analysis of ion engine discharge cathode keeper, *J. Propul. Power* 21 (2005) 102–110, <https://doi.org/10.2514/1.4441>.
- [14] D.C. Byers, A. Snyder, Parametric investigation of mercury hollow-cathode neutralizers, *J. Spacecraft Rockets* 8 (1971) 133–139, <https://doi.org/10.2514/3.30233>.
- [15] T. Meng, Z. Ning, D. Yu, Triggering of ionization oscillations in hollow cathode discharge by keeper electrode, *Phys. Plasmas* 26 (2019), 093510, <https://doi.org/10.1063/1.5116830>.
- [16] D. Pedrini, R. Albertoni, F. Paganucci, M. Andrenucci, Modeling of LaB6 hollow cathode performance and lifetime, *Acta Astronaut.* 106 (2015) 170–178, <https://doi.org/10.1016/j.actaastro.2014.10.033>.
- [17] M. Omrani, R. Amrollahi, D. Iraji, Experimental measurements of the hollow cathode DC glow discharge parameters in Ar and He plasmas, *Plasma Sources Sci. Technol.* 25 (2016), 065011, <https://doi.org/10.1088/0963-0252/25/6/065011>.
- [18] Y. Qin, K. Xie, N. Guo, Z. Zhang, C. Zhang, Z. Gu, Y. Zhang, Z. Jiang, J. Ouyang, The analysis of high amplitude of potential oscillations near the hollow cathode of ion thruster, *Acta Astronaut.* 134 (2017) 265–277, <https://doi.org/10.1016/j.actaastro.2017.02.012>.
- [19] D.R. Lev, I.G. Mikellides, D. Pedrini, D.M. Goebel, B.A. Jorns, M.S. McDonald, Recent progress in research and development of hollow cathodes for electric propulsion, *Rev. Mod. Plasma Phys.* 3 (2019) 6, <https://doi.org/10.1007/s41614-019-0026-0>.
- [20] B.A. Jorns, I.G. Mikellides, D.M. Goebel, Ion acoustic turbulence in a 100-A LaB6 hollow cathode, *Phys. Rev. E* 90 (2014), 063106, <https://doi.org/10.1103/PhysRevE.90.063106>.

- [21] B.A. Jorns, C. Dodson, D.M. Goebel, R. Wirz, Propagation of ion acoustic wave energy in the plume of a high-current LaB<sub>6</sub> hollow cathode, Phys. Rev. E. 96 (2017), 023208, <https://doi.org/10.1103/PhysRevE.96.023208>.
- [22] Q. Xia, K. Xie, N. Wang, Discharge characteristics of cathodic hollow-cathode plasma contactors and related similarity to ground simulations, Vacuum 169 (2019), 108870, <https://doi.org/10.1016/j.vacuum.2019.108870>.
- [23] J.D. Williams, P.J. Wilbur, Experimental study of plasma contactor phenomena, J. Spacecraft Rockets 27 (1990) 634–641, <https://doi.org/10.2514/3.26192>.
- [24] J.D. Williams, P.J. Wilbur, Electron emission from a hollow cathode-based plasma contactor, J. Spacecraft Rockets 29 (1992) 820–829, <https://doi.org/10.2514/3.25537>.
- [25] D.E. Parks, I. Katz, B. Buchholtz, P. Wilbur, Expansion and electron emission characteristics of a hollow-cathode plasma contactor, J. Appl. Phys. 74 (1993) 7094–7100, <https://doi.org/10.1063/1.355023>.
- [26] J.E. Hansen, W. Persson, Revised analysis of singly ionized xenon, Xe II, Phys. Scripta 36 (1987) 602, <https://doi.org/10.1088/0031-8949/36/4/005>.
- [27] J.D. Williams, P.J. Wilbur, Electron emission from a hollow cathode-based plasma contactor, J. Spacecraft Rockets 29 (1992) 820–829, <https://doi.org/10.2514/3.25537>.
- [28] E.Y. Choueiri, Plasma oscillations in Hall thrusters, Phys. Plasmas 8 (2001) 1411–1426, <https://doi.org/10.1063/1.1354644>.
- [29] M.P. Georgan, B.A. Jorns, A.D. Gallimore, An experimental and theoretical study of hollow cathode plume mode oscillations, in: 35rd International Electric Propulsion Conference, 2017. [https://www.electricrocket.org/IEPC\\_Master\\_List.html#2017](https://www.electricrocket.org/IEPC_Master_List.html#2017).
- [30] M.P. Georgan, B.A. Jorns, A. Gallimore, Plasma instabilities in the plume of a hollow cathode, in: Joint Propulsion Conference, American Institute of Aeronautics and Astronautics, 2018, <https://doi.org/10.2514/6.2018-4427>.
- [31] K. Xie, F. Tian, F. Liang, Q. Xia, N. Wang, Discharge instability in a plasma contactor, Plasma Sci. Technol. 22 (2020). <https://iopscience.iop.org/article/10.1088/2058-6272/ab9bf9>.
- [32] B.A. Jorns, I.G. Mikellides, D.A. Goebel, A. Lopez Ortega, Mitigation of energetic ions and keeper erosion in a high-current hollow cathode, in: 34th International Electric Propulsion Conference, Hyogo-Kobe, Japan, 2015. [https://www.electricrocket.org/IEPC\\_Master\\_List.html#2015\\_INDEX](https://www.electricrocket.org/IEPC_Master_List.html#2015_INDEX).
- [33] N. Yanes, B. Jorns, A. Friss, J.E. Polk, P. Guerrero, J.M. Austin, Ion acoustic turbulence and ion energy measurements in the plume of the HERMeS thruster hollow cathode, in: 52nd AIAA/SAE/ASEE Joint Propulsion Conference, American Institute of Aeronautics and Astronautics, 2016, <https://doi.org/10.2514/6.2016-5028>.
- [34] D.M. Goebel, I. Katz, Fundamentals of Electric Propulsion: Ion and Hall Thrusters, 2008, <https://doi.org/10.1002/9780470436448>.
- [35] A.N. Grubisic, S.B. Gabriel, Assessment of the T5 and T6 hollow cathodes as reaction control thrusters, J. Propul. Power 32 (2016) 810–820, <https://doi.org/10.2514/1.B35556>.